Journal of Atmospheric and Solar–Terrestrial Physics 196 (2019) 105148

Contents lists available at ScienceDirect

Journal of Atmospheric and Solar-Terrestrial Physics

journal homepage: www.elsevier.com/locate/jastp

Research Paper

Evaluation of estimated mesospheric temperatures from 11-year meteor radar datasets of King Sejong Station (62°S, 59°W) and Esrange (68°N, 21°E)

Hosik Kam [a,c], Yong Ha Kim [a,*], Nicholas J Mitchell [b], Jeong-Han Kim [c], Changsup Lee [c]

[a] Department of Astronomy, Space Science and Geology, Chungnam National University, Daejeon, South Korea
[b] Department of Electronic & Electrical Engineering, University of Bath, Bath, UK
[c] Division of Polar Climate Sciences, Korea Polar Research Institute, Incheon, South Korea

ARTICLE INFO

Keywords:
Mesospheric temperatures
Meteor radar
Ambipolar diffusion
King Sejong Station
Esrange

ABSTRACT

We have evaluated the reliability of two methods for estimating mesospheric temperatures from all-sky VHF meteor radar data. The first method utilizes the decay time of meteor trails, and the other method takes advantage of the linear relation between temperatures and the full width at half maximum (FWHM) of the observed meteor echoes height distribution. We estimated the temperatures from two meteor radar datasets of King Sejong Station (62.22°S, 58.78°W), Antarctic and Esrange, Sweden (67.90°N, 21.10°E) during a period of 2007–2017 and 2003 to 2013, respectively. We devised an improved decay time method of temperature estimation that utilizes careful selection of detected echoes by reflecting seasonal change in height range where ambipolar diffusion is dominant in meteor decay. Applying the improved method, we achieved temperature estimation on average within 6.2 and 5.4% from Aura/MLS temperatures around 90 km at Esrange and KSS, respectively. In comparison, temperatures estimated by the FWHM method have mean differences of 5.1 and 3.6% from the MLS temperatures at Esrange and KSS, respectively. The FWHM temperatures show significantly less discrepancy from MLS temperatures and temporal fluctuations than the temperatures estimated by the decay time for both sites. This may indicate that the FWHM method is more robust to estimate mesospheric temperatures from meteor radar data.

1. Introduction

Meteor radars (MRs) have been used around the world to study neutral dynamics in the mesosphere and lower thermosphere (MLT) region for decades. MRs are well suited to monitor the variation of mesospheric temperatures continuously day and night, unlike other ground-based optical instruments which are affected by weather conditions. By analyzing the VHF signal backscattered from meteor plasma trails, MRs can estimate winds and temperatures of the background atmosphere in the MLT region. In particular, meteor trails are mostly detected in the altitude range of 70–100 km by MR, and are decayed by various processes such as ambipolar diffusion, recombination, and chemical interaction (e.g. Baggaley and Cummack, 1974; Chilson et al., 1996; Cervara and Reid, 2000; Ballinger et al., 2008; Kim et al., 2010; Lee et al., 2013; Younger et al., 2008, 2014). Previous studies noted that the meteor decay time depends mostly on ambipolar diffusion and its coefficient is a function of atmospheric pressure and temperature (Jones, 1991; Hocking et al., 1997, 2004; Singer et al., 2003; Holdsworth et al., 2006; Stober et al., 2008; Kim et al., 2012; Meek et al., 2013; Kozlovsky et al., 2016; Yi et al., 2016; Lima et al., 2018). However, several studies have pointed out that the behaviors of decay time height profiles are significantly different for seasons and electron line densities in meteor trails (Younger et al., 2008; Kim et al., 2010, 2012; Lee et al., 2013). Hence, it seems necessary to consider the variation of decay time height profiles with seasons in the process of temperature estimation.

Since Hocking (1999) proposed the technique of mesospheric temperature estimation without pressure information, instead, using the vertical temperature gradient and decay time of backscattered meteor echo, a number of studies have been dedicating to improve and validate the estimated temperatures by applying their own criteria. Some of previous reports (Dyrland et al., 2010; Hall et al., 2006, 2012; Holmen et al., 2016) showed that derived daily temperatures from meteor decay

* Corresponding author.
E-mail address: yhkim@cnu.ac.kr (Y.H. Kim).

https://doi.org/10.1016/j.jastp.2019.105148
Received 17 March 2019; Received in revised form 7 October 2019; Accepted 8 October 2019
Available online 11 October 2019

times are significantly different from those of satellite observation by up to ~100 K. Holdsworth et al. (2006) have used gradient and pressure techniques and have recommended the use of the pressure method instead of gradient method. Meek et al. (2013) have compared the meteor radar temperature by gradient and pressure methods at 80 °N with those measured by Microwave Limb Sounder (MLS) on Aura satellite. Recently, Lima et al. (2018) have used meteor radar observations to estimate the mesospheric temperatures at 90 km at low latitude sites in the southern hemisphere, by applying gradient and pressure methods and compared with those of Sounding of the Atmosphere using Broadband Emission Radiometry (SABER) instrument on board the Thermosphere Ionosphere Mesosphere Energetics and Dynamics (TIMED) satellite. In order to improve the quality of temperature estimation from meteor decay times, Kim et al. (2010, 2012) proposed that among underdense meteor echoes only weak meteor echoes, defined as the lower quartile in the distribution of relative electron line densities, should be used in temperature estimation. The low line density trails are primarily decayed by ambipolar diffusion, whereas high line density trails are controlled by not only the diffusion but also by other processes such as chemical recombination and non-uniform dissipation. Kim et al. (2012) argued that estimated monthly mean temperatures from only weak echoes agreed significantly better with satellite observation.

Recently, Lee et al. (2016) suggested a new method to estimate the mesospheric temperatures from meteor echo data. They found that the vertical gradient of background atmospheric pressure is linearly correlated with the full width at half maximum (FWHM) in height distribution of meteor echoes detected by MR. Liu et al. (2017) also used the FWHM for estimating temperature at 53°N, based on SABER temperatures. The new method utilizes the linear relationship between the FWHM of meteor height distribution and the atmospheric pressure gradient.

In this paper, we evaluate two methods (gradient and FWHM) of estimating mesospheric temperatures by applying those methods to the datasets observed at Esrange, Sweden (67.90°N, 21.10°E) during 2003–2013 and King Sejong Station, Antarctica (62.22° S, 58.78°W) during 2007–2017. The estimated temperatures are compared with independent temperatures measured by space-born instrument. We also discuss the ways of improving temperature estimation in both methods.

2. Instruments

We used two MRs for estimating the mesospheric temperatures over Northern and Southern high latitude regions. One of the MRs has been operated at Antarctic King Sejong Station (hereafter; KSS) since March 2007 by Korea Polar Research Institute (KOPRI) and Chungnam National University, and is manufactured by ATRAD. Another MR is located at Esrange, Sweden and produced by SKiYmet. The KSS MR is configured at a central frequency of 33.2 MHz with pulse repetition frequency (PRF) of 440 Hz and the Esrange MR is operated by the central frequency of 32.5 MHz with PRF of 2144 Hz. Both MRs are composed of one transmitter antenna (Tx) and five receiver antennae (Rx1~Rx5), and Rx antennae form an interferometric array with centering on Rx1 between two baselines. Each Rx antenna is arranged in a direction parallel to the Rx antennae array with a reflector element and a driven element consisting of a T-matched cross dipole. The KSS MR's Tx antenna transmitted with the peak power of 8 kW until January 2012 and it was upgraded to 12 kW in February 2012 and that of Esrange MR's Tx is 6 kW. The total daily number of meteor detection ranges 15,000–40,000 and 5000–15,000 from the KSS and the Esrange, respectively. The daily counts of meteor echo show clear seasonal variation with a maximum in summer and minimum in winter except the periods before 2009 for KSS and after 2009 for Esrange, as shown in Fig. 1. The echo detection rate in the KSS has increased since 2012 due to the upgrade of transmission power and the reduction of background noise (Jee et al., 2014). The Esrange MR didn't operate in winter of 2009/2010 because of a hardware problem, after which the radar has not fully operated, resulting in decrease in the meteor detection count and not showing the seasonal variation.

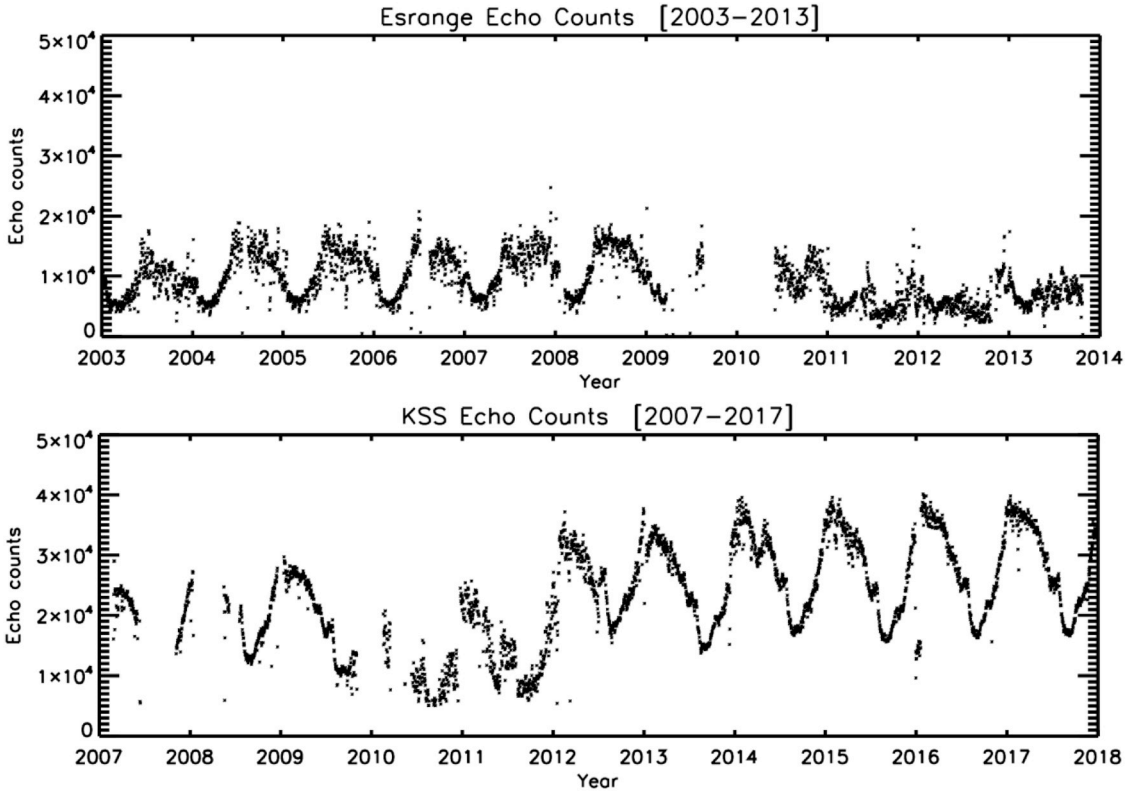

Fig. 1. Daily meteor echo counts at Esrange (top) for 2003–2013 and KSS (bottom) for 2007–2017.

For comparison with estimated temperatures from MR, the temperatures and geopotential heights (GPH) data were obtained from NASA/Aura satellite over KSS and Esrange. The satellite was launched on July 15, 2004, and Microwave Limb Sounder (MLS) loaded on the NASA/Aura has been observing Earth's atmosphere as vertical structure of atmospheric gases, temperatures, pressure, and ice particles from the surface to an altitude of 90 km since August 13, 2004 (Schwartz et al., 2008). The satellite has an orbital inclination of 98° and is in a Sun-synchronous polar orbit at an altitude of 705 km, and thus can cover daily global regions up to northern and southern high latitudes. In this study, we restricted MLS data to the 5° by 5° grid in longitude and latitude centered at each MR site for a direct comparison with temperatures from the MRs. The entire MLS GPH values were converted into geometric heights and MLS temperatures were interpolated at 90 km for the comparison.

3. Meteor echo selection for temperature estimation

Since the two temperature estimation methods in this study utilize completely different parameters of meteor echoes, we need to choose suitable samples of meteor echoes, based on physical parameters. Both temperature estimation methods rejected meteor echoes with zenith angles greater than 70° because those echoes suffer from interferometry issues because of the signal traveling close to the ground. We also excluded meteor echoes with signal-to-noise ratio (SNR) less than 7.4 dB because their signals are too weak to determine useful information (Kim et al., 2012). It has been known that the meteors during a meteor shower have significantly different physical properties compared to those of sporadic meteors. Although total count of shower meteors per day might be relatively smaller than that of sporadic meteors, these could affect the meteor distributions and decay time profiles with height. Hence, in order to reduce the effect by shower meteors, we excluded the echoes with the speed over 35 km/s based on the studies by Younger et al., 2009 and Schult et al. (2018), which summarized the physical parameters of meteor showers for the locations of southern and northern high latitudes, respectively. In addition, for Esrange we excluded meteor echoes with the location ambiguity tag of SKiYmet, which comprise about 10% of detected echoes.

For the temperature estimation from the FWHM, the accuracy of height information of each echo is the most important factor. Since phase differences between antenna pairs are used for determining the azimuth and zenith angles, the error in phase differences should be low enough to estimate the accurate height information. Signals from other active instruments close to the MR may act as noise sources and probably increase the phase error between receiver antenna pairs. The meteor radar at Esrange gives only the worst phase error between antenna pairs for each echo, whereas the meteor radar at KSS provides a mean phase error of all antenna pairs. Fig. 2 shows distributions of the worst phase errors for Esrange meteor echoes (top), and distributions of mean phase error for KSS meteor echoes (bottom). The phase error distributions of the Esrange radar below 80 km (left) and above 100 km (right) drastically increase from 20°, whereas the distribution for the 80–100 km range (center) peaked around 15°. Hocking (2004) noted that the phase error larger than 25° may cause a serious problem for determining the location of meteor echo. Thus, Fig. 2 indicates that the majority of Esrange meteor echoes below 80 km and above 100 km may have critical errors in their height information. In our analysis the meteor echoes with the worst phase error larger than 20° are excluded. In case of KSS MR (Fig. 2 bottom), all the distributions of mean phase errors have a peak at 0° with a narrow width, implying the reasonable accuracy in meteor heights. In addition, the height accuracy may also be affected by pulse length and pulse coding method. To be safe, we use KSS

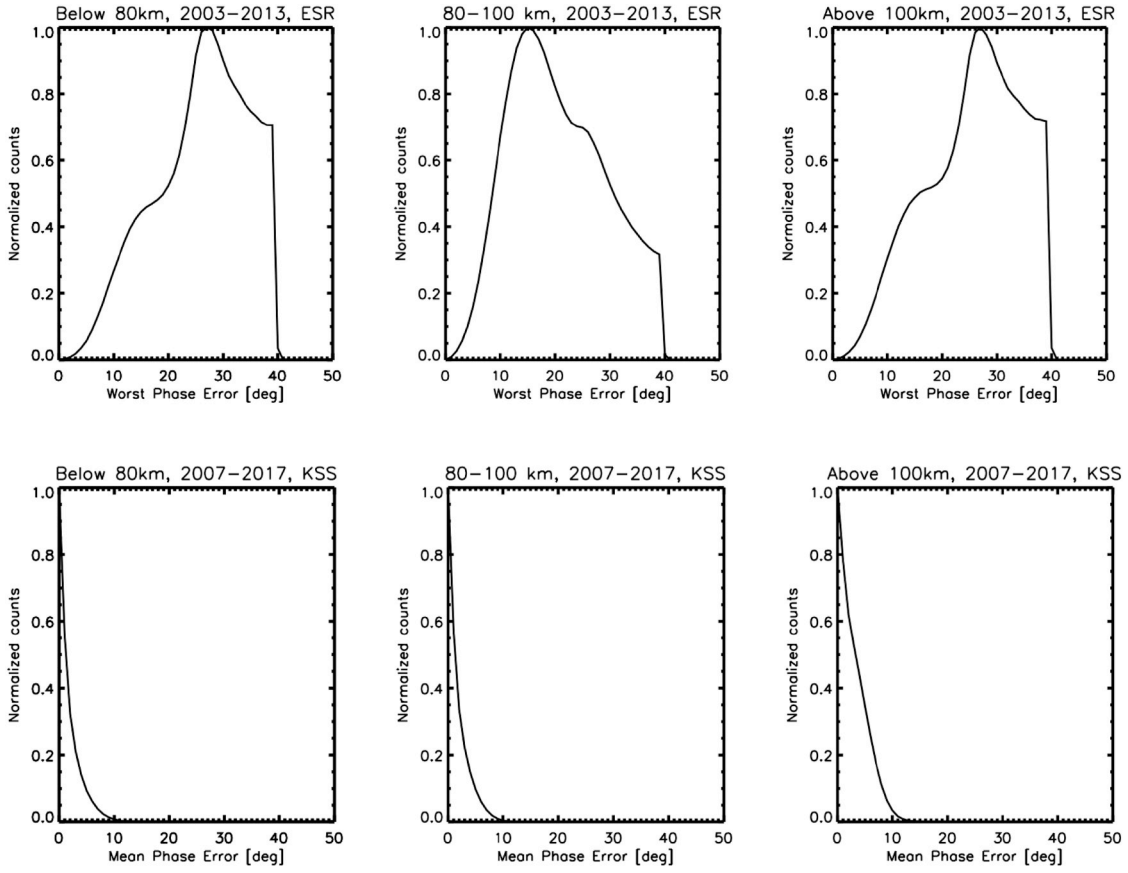

Fig. 2. Distributions of worst phase errors at Esrange (top) and distributions of mean phase errors at KSS (bottom) for meteor echoes below 80 km (left), 80 km–100km (center), and above 100 km (right) in the whole data set of 11 years.

echoes with the mean phase error less than 6°.

In the case of the meteor decay time method, we used only weak echoes among the detected underdense meteor echo, defined as lower quartile in the distribution of relative electron line densities computed from the received powers and ranges of echoes. Weak echoes are dissipated efficiently by ambipolar diffusion according to the background atmospheric pressure and temperature. MRs determine the decay time of meteor trail defined as a time duration from the maximum amplitude of signal to 1/e of the maximum amplitude. Based on the assumption that the meteor decay time is determined solely by ambipolar diffusion, the mesospheric temperatures (T) can be computed by Eq. (1) (Hocking, 1999; Kim et al., 2012),

$$T = S\left(2T_g + \frac{mg}{k}\right) log_{10} e \quad (1)$$

where m is the mass of atmospheric molecules, g is the gravitational constant, and k is Boltzmann constant, T_g is atmospheric temperature gradient, and S is the slope in a plot of height versus log inversed decay time (LIDT). We adopted the temperature gradient model (T_g) from Kim et al. (2012) for KSS and from Hocking et al. (2004) for Esrange. The temperature gradients are in the range of −3 ∼+3 K/km and −4 ∼ +2 K/km, varying with season, for Esrange and KSS, respectively. Since the temperature gradient value is model-dependent, it is a source of uncertainty in the decay time method.

For calculating the slope S, we need to define a height range where ambipolar diffusion is dominant in the decay process of meteor trails. Most of previous studies utilized a fixed height range from 85 km (or 86 km for KSS) to 95 km and thus ignored the seasonal variation in height structure of meteor decay time. At the altitudes below 85 km, the decay time is significantly affected by dust particles and electron recombination process (Hall et al., 2006; Ballinger et al., 2008; Younger et al., 2008; Kim et al., 2010, 2012). Above 95 km altitude, the motion of electron in the meteor trail is restricted by geomagnetic field line due to low neutral density (Jones, 1991; Dyrud et al., 2001; Hocking, 2004; Kim et al., 2012). Hence, the slope of decay time profile can be reversed in these altitude ranges, and thus temperature estimation from ambipolar diffusion should be restricted to the altitude region between the two limiting altitudes: high neutral density at lower altitudes primarily controls chemical reactions while rare atmospheric density at higher altitudes allows geo-magnetic field to inhibit the diffusion of meteor plasma trail. Fig. 3 shows height distributions of LIDT of meteor echoes and histograms of meteor echoes on a specific day in summer (left) and winter (right). It is evident from Fig. 3 that the height range of the ambipolar diffusion dominant region (hereafter main stream) should be defined differently by reflecting the seasonal variation of decay time. We found that the lower boundary of the main stream reaches up to 87 km altitude in summer and down to 83 km in winter. Previous studies, using a fixed height range of the main stream between 85 and 95 km, severely overestimated mesospheric temperatures in summer due to inclusion below the actual lower boundary of the main stream. In summer, the main stream of detected echoes, defined as those within the FWHM of height distribution (indicated as red solid line in Fig. 3) is bounded by a narrower height range due to cooler atmosphere than in winter, as shown in Fig. 3. Meteor echoes located near or outside the lower boundary are affected by chemical reactions with background atmospheric molecules in addition to ambipolar diffusion, resulting in shorter decay times (larger inverse decay time and larger effective diffusion coefficient). This leads to increase the slope of diffusion coefficient, S in Eq. (1), and thus overestimate mesospheric temperatures. Therefore, the seasonal changes in neutral density need to be considered before

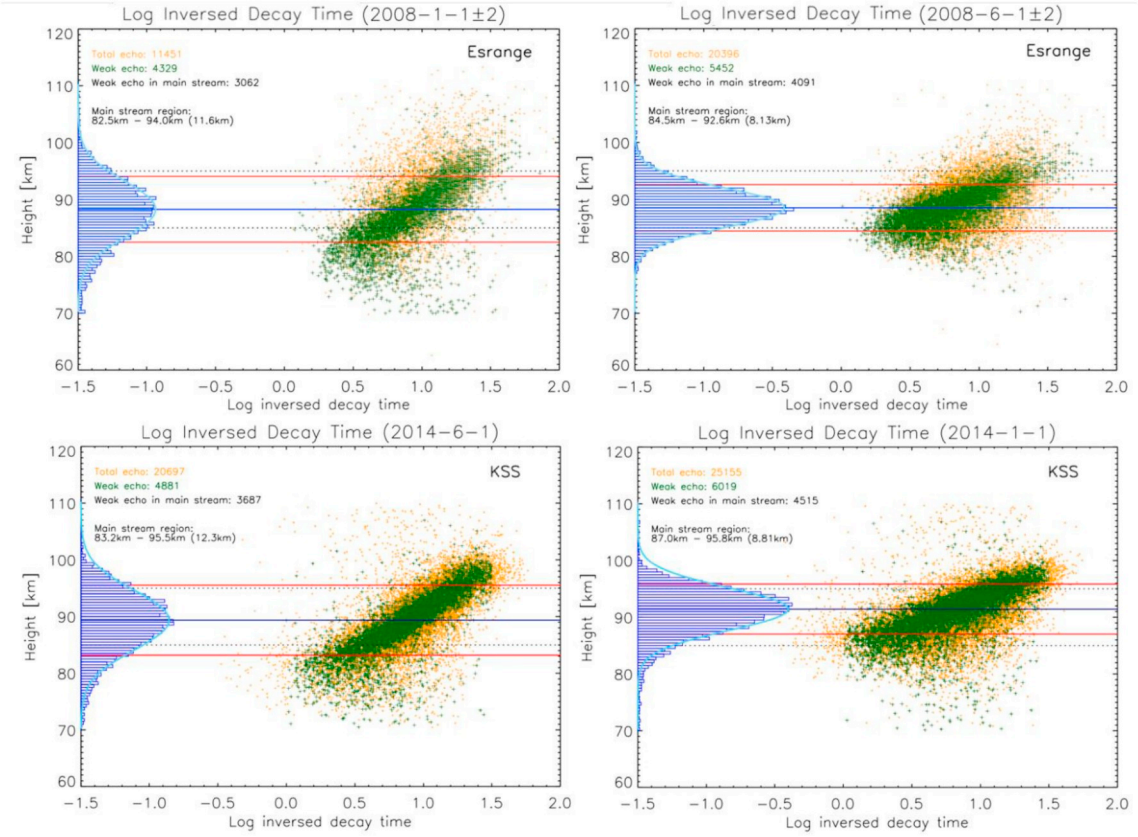

Fig. 3. Height distributions of log inversed decay times for 5-day accumulated echoes in winter (left) and summer (right) at Esrange (top) and for daily observed echoes at KSS (bottom). Histograms (blue) on the left vertical axis indicate the height distribution of weak echoes, sky lines are Gaussian fitting lines for each histogram. Navy and red lines are peak heights and heights of FWHM, respectively. Dotted lines indicate the traditional height range, whereas red lines indicate the main stream height range, for determining the slope of meteor decay times.

correctly computing the slope of decay time versus the height for temperature estimation. Thus, we choose the altitude range by reflecting seasonal variations in the atmospheric density, instead of using a fixed height range.

According to Lee et al. (2016), the FWHM of a meteor height distribution is proportional to the gradient of atmospheric pressures, which can be described in terms of the geopotential heights and two fundamental equations such as ideal gas law, and hydrostatic equilibrium equation. Then, the difference in geopotential heights of lower and upper altitudes corresponding to the FWHM is expressed as

$$Z_2 - Z_1 = \frac{R}{g} < T > \ln\left(\frac{P_1}{P_2}\right) \quad (2)$$

where P_1 and P_2 are atmospheric pressure at Z_1 and Z_2, respectively, and g is the gravitational acceleration as 9.5 m/s^2 at MLT region and R is the gas constant as 287.05 J/kg/K. The layer mean temperature can be defined as averaged value of temperature between Z_1 and Z_2. Consequently, after rearranging Eq. (2), the linear relationship between the FWHM ($Z_2 - Z_1$) and the layer mean temperature is expressed by

$$T = C \cdot FWHM \quad (3)$$

where C is $\frac{g}{R}\left[\ln\left(\frac{P_1}{P_2}\right)\right]^{-1}$. Instead of calculating C from an atmospheric model, Lee et al. (2016) regarded it as the slope of the notable linear relationship between the daily FWHM versus MLS temperature at 90 km, which they found high correlation coefficients.

Here, we verify their claim of high correlation by independently analyzing the dataset from KSS and Esrange for 11 years. The FWHM of meteor echo height distribution was derived by Gaussian-fitting the single day distribution of meteor echoes, as shown in Fig. 4. The Gaussian-fitting also generates a meteor peak height (MPH) as a maximum of the distribution. We used the height range of 70–110 km for KSS MR and 80–100 km for Esrange MR that has the lower meteor detection rate. We note that most of Esrange meteor echoes beyond the 80–100 km altitude range (pink shades in Fig. 4) have large phase errors, having significantly different distributions from those between 80 and 100 km as shown in Fig. 2. Accordingly, we only used Esrange meteor echoes between 80 and 100 km altitude in this study, because the unordinary distribution of meteor counts beyond the 80–100 km range cannot be accurately identified. About 20,000 echoes are needed to determine the FWHM within the accuracy of 2% so that Esrange meteor counts were accumulated to derive FWHM for 5 day as in Fig. 4.

Following Eq. (3), we examine the relation between FWHMs and MLS temperatures for each year, and examples of scatter plots for the relation are shown in Fig. 5. Table 1 summarizes the correlation coefficients and slopes of the linear relation between FWHMs and MLS temperatures. The correlation coefficients are indeed sufficiently high, ranging from 0.80 to 0.95 with a mean value of 0.88 for Esrange (left) and from 0.77 to 0.95 with a mean value of 0.92 for KSS (right). For KSS, the entire period except 2009, when mechanical problems occurred on the KSS MR, the average value of correlation coefficient between the FWHM and MLS temperature is 0.93. Before excluding the echoes with higher phase error, the averaged correlation coefficients for 11 years between FWHM and MLS temperatures are 0.86 and 0.90 for Esrange and KSS, respectively. In other words, the higher phase error interrupted to correctly determine the FWHM of echo height distribution. The proportionality constant, C, slightly varies with year from 14.80 to 15.54 (standard deviation of 0.23) for Esrange and from 15.97 to 16.91 (standard deviation of 0.27) for KSS, respectively. The difference of slopes between the two sites probably originates from different instrumental properties and latitudes. Assuming that incoming meteors do not vary from one year to another, we selected the constant C value of 2013 as the representative C value (15.13 for Esrange and 16.66 for KSS) for the linear relation, based on the largest correlation coefficients in both sites. Especially, Lee et al. (2018) examined the C value from a linear relationship between KSS MR and SABER temperatures from 2012 to 2016, and their 5-year averaged C is 16.68 ± 0.26, which is close to our

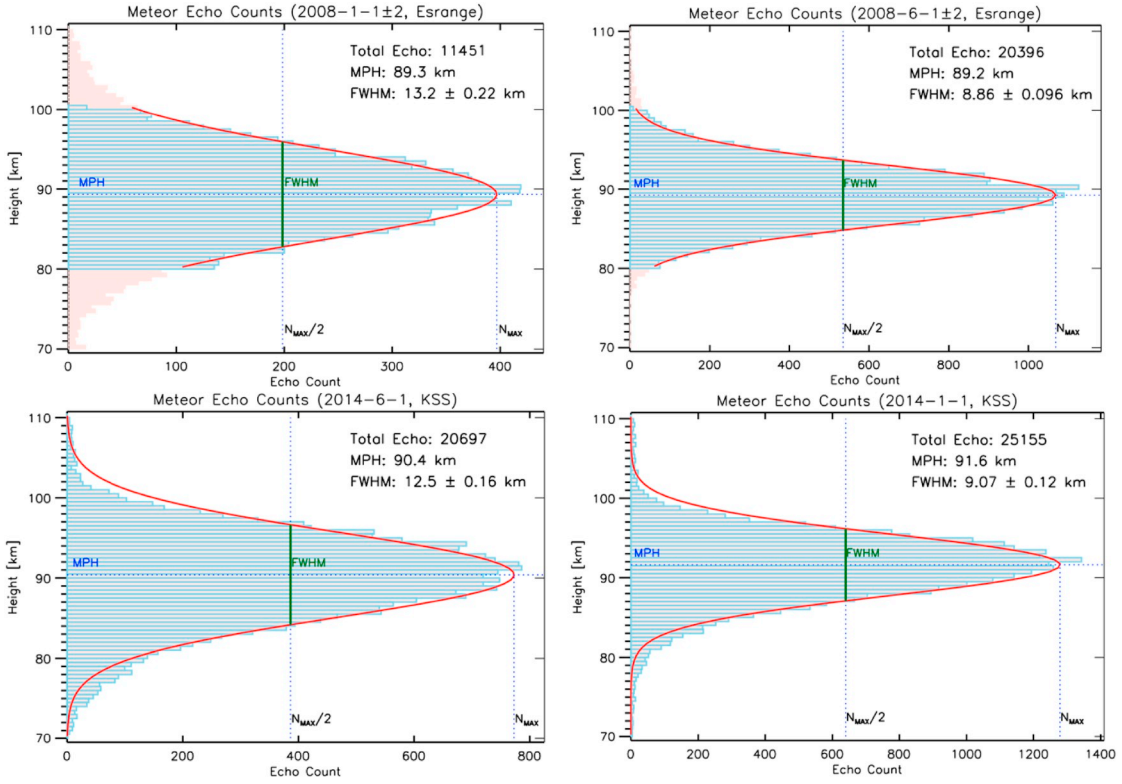

Fig. 4. Height distributions of 5-day accumulated meteors at Esrange (top) and of daily observed meteors at KSS (bottom) in winter (left) and summer (right). The vertical resolution of histograms is 0.5 km and MPH (horizon blue dashed lines) is calculated from Gaussian fitting (red lines) for each distribution.

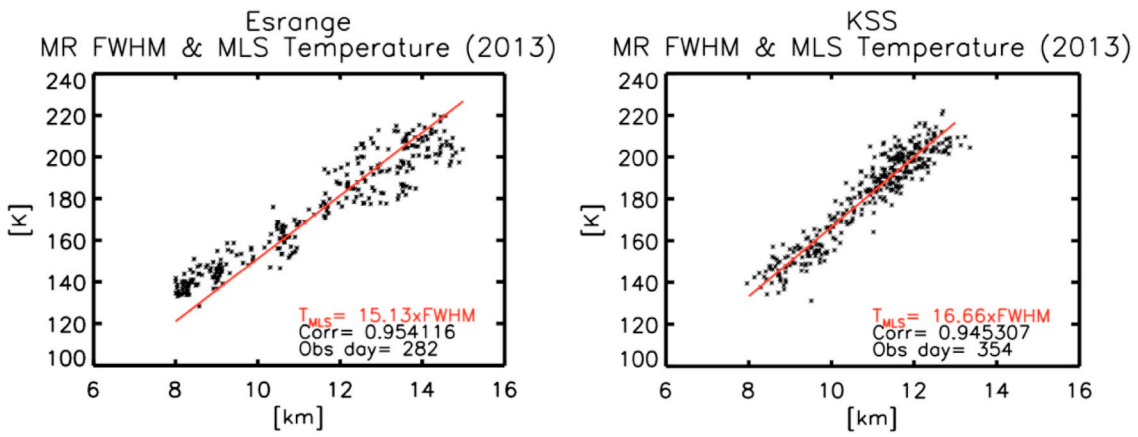

Fig. 5. Examples of scatter plots between MLS temperatures at 90 km and FWHM over Esrange (left) and KSS (right) for the year 2013.

Table 1
Correlation parameters between the FWHMs and MLS temperatures at Esrange and KSS.

Esrange			KSS		
Year	Correlation Coefficient	Slope	Year	Correlation Coefficient	Slope
2003	–	–	2007	0.92	16.91 ± 0.55
2004	0.80	15.17 ± 0.54	2008	0.93	16.60 ± 0.46
2005	0.86	15.38 ± 0.47	2009	0.77	16.17 ± 0.66
2006	0.87	14.80 ± 0.45	2010	0.90	16.33 ± 0.52
2007	0.93	15.54 ± 0.45	2011	0.91	15.97 ± 0.38
2008	0.81	15.51 ± 0.58	2012	0.93	16.60 ± 0.38
2009	0.92	15.33 ± 0.29	2013	0.95	16.66 ± 0.31
2010	0.92	15.16 ± 0.50	2014	0.95	16.62 ± 0.32
2011	0.91	15.34 ± 0.35	2015	0.94	16.65 ± 0.32
2012	0.86	15.02 ± 0.37	2016	0.93	16.56 ± 0.38
2013	0.95	15.13 ± 0.36	2017	0.93	16.74 ± 0.34
Mean	0.88	15.24 ± 0.46	Mean	0.92	16.52 ± 0.42

C value despite the different satellite dataset.

The apparent constant relation between FWHM and temperatures is the consequence of atmospheric expansion or contraction while the incoming meteor characteristics are fairly constant, perhaps except some meteor shower events. This assertion has been fully tested during the publication process of Lee et al. (2016). Stober et al. (2011) computed a meteor ablation model, which suggests that the meteor mass distribution is more strongly affecting the meteor height distribution than the incoming velocities. Sporadic meteors seem to have a fairly constant mass distribution year by year. The detail meteor ablation processes are beyond the scope of the current study.

4. Temperature evaluation

The overall procedure for temperature estimation from observed decay times by using Eq. (1) is identical to that in Kim et al. (2012). Estimated daily temperatures are shown as red dots in Fig. 6, and MLS temperatures at 90 km (green dots) are presented for comparison. Using each representative C in Eq. (3), we also estimated temperatures from derived FWHMs of meteor height distributions for each site. The FWHM temperatures are plotted with black dots in Fig. 6. Although all the temperatures in Fig. 6 show clear seasonal variations and good agreement each other, temperatures estimated from MR data by both methods have larger day-to-day fluctuations than the MLS temperatures, especially in winter. The 11-year root mean square (RMS) differences between the FWHM and MLS temperatures are 5.1 ± 3.8% for Esrange and 3.6 ± 3.0% for KSS, while the RMS differences between temperatures from decay times and MLS temperatures are 6.2 ± 4.9% and 5.4 ± 4.1% at Esrange and KSS, respectively. Before applying the meteor echo selection criteria (no exclusion of echoes with high phase error), RMS differences between FWHM and MLS temperatures are 5.8 ± 3.6% and 4.3 ± 3.0% at Esrange and KSS, respectively. The estimated FWHMs including high phase error echoes lead to not only lower correlation coefficients but also slightly higher RMS differences from MLS temperatures. In addition, when echoes within the traditional fixed height range (86–95 km) were used for deriving the slope, S, of LIDT, RMS differences between decay time temperatures and MLS temperatures show 6.8 ± 4.2% and 6.6 ± 4.9% at Esrange and KSS, respectively, worse than the current results. Thus, seasonally varying height ranges should be considered in determining the slope S. For both sites, the FWHM method provides more stable and consistent temperatures than the decay time method over the entire observation period. The seemingly abnormal echo counts at Esrange after 2011, as shown in Fig. 1, do not seem to affect much the quality in temperature estimation for both methods, because the Esrange data were accumulated for five days.

Fig. 7 shows monthly averaged relative differences of FWHM temperatures and decay time temperatures from MLS temperatures for the 11 year periods. The decay time temperature differences (ΔT_{DC}) at Esrange seem to still overestimate except winter when estimated slopes were rarely interrupted by lower boundary of the main stream. In contrast, both temperature differences at KSS stay within ~5%. Although we obtained improved temperatures from decay times by using the height ranges of the main stream, which reflects the seasonal variation in background atmospheric density, the standard deviations of the temperature differences seem to be persistently larger for decay-time temperatures than FWHM temperatures for both sites (bottom panels of Fig. 7). In other words, the FWHM temperatures have not only smaller overall differences from MLS temperatures but also smaller standard deviations throughout seasons than the decay temperatures.

The decay time method has a fundamental source of uncertainty in T_g of eq (1): 2 T_g, comparing with mg/k, contributes to the estimated temperature as much as 20%, so that a 10% of uncertainty in T_g may cause about 2% uncertainty in the temperature. More critical uncertainty is from determination of the slope, S, which is affected sensitively by selecting the height range and weak echoes, as shown in Fig. 3. We have mitigated this uncertainty by using varying height ranges with season and selecting weak echoes in low quartile of electron line densities. On the other hand, the FWHM method is rather robust to determine FWHM values from meteor height distribution: 1.5% accuracy of FWHM is usually achieved as shown in Fig. 4. Main source of uncertainty in the FWHM temperatures is from the correlation uncertainty between FWHM's and temperatures. The perfect correlation requires an assumption that the height distribution of detected echoes depend solely on mesospheric temperatures, not affected by variation of incoming meteor characteristics. Since the slopes between FWHM and MLS temperatures are fairly constant year by year as shown in Table 1, the

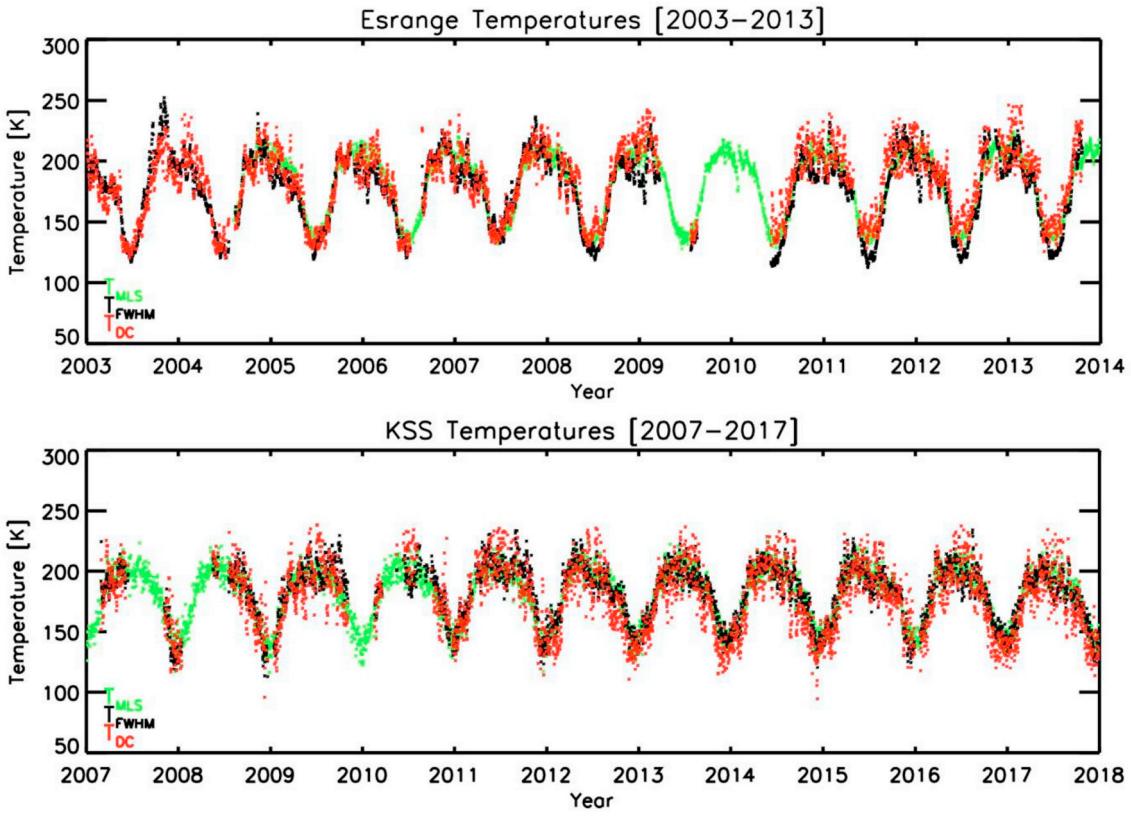

Fig. 6. Estimated temperature from FWHM (black dots) and decay time (red dots) are compared with MLS temperatures at 90 km (green dots) for the periods of 11 years at Esrange (top) and KSS (bottom).

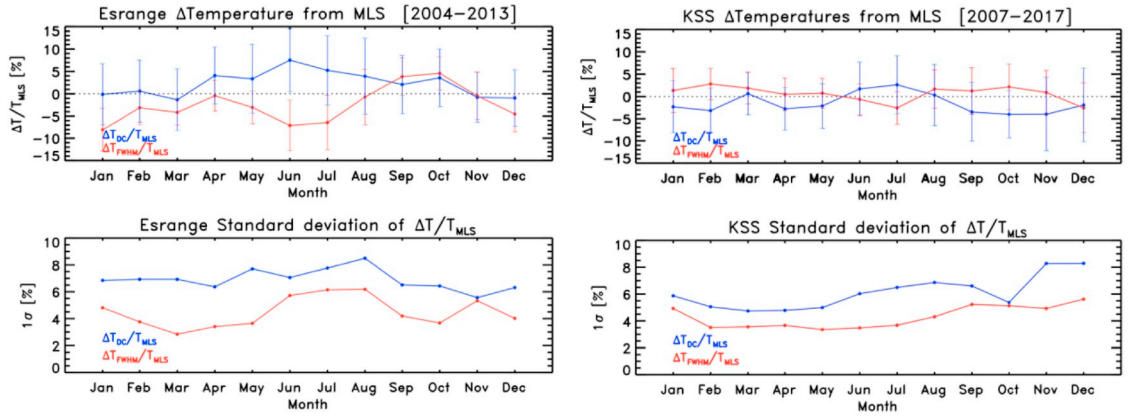

Fig. 7. Averaged percentage differences of FWHM temperatures and decay-time temperatures from MLS temperatures (top) for the 11 year periods of Esrange (left) and KSS (right) observations. The corresponding standard deviations (bottom).

assumption seems justified in a practical sense. Fig. 7 clearly shows the practical advantage of the FWHM method, compared with the decay time method. The effects of variation in meteor characteristics on the height distribution need to be studied in other investigations.

5. Summary and conclusion

By comparing with MLS temperature measurements, we examined two different methods of mesospheric temperature estimation from meteor radar data; the meteor decay time and the height width (FWHM) of meteor distribution. We applied the two methods to 11-year meteor radar data from Esrange and King Sejong Station (KSS), as Northern and Southern high latitude sites. In an effort to improve the accuracy in both methods, we excluded meteor echoes with high phase errors. The spatial information of detected meteor echoes can be more precisely determined by selecting echoes with low phase errors of the received signal and within the optimal ranges of zenith angles and distances. In the decay time method, we used only the weak echoes observed within the varying height ranges with season. Applying the new meteor echo selecting process to the decay time method, we achieved temperature estimation on average within 6.2 and 5.4% (10.9 and 10.7 K) from Aura/MLS temperatures at 90 km at Esrange and KSS, respectively. Temperatures estimated by the FWHM method have averaged differences of 5.1 and 3.6% (9.5 and 7.0 K) from the MLS temperatures at Esrange and KSS, respectively. The FWHM temperatures show significantly less fluctuation and smaller standard deviations from MLS temperatures

than the temperatures estimated by the decay time for both sites. Therefore, we conclude that the FWHM method is more robust to estimate mesospheric temperatures from meteor radar data.

Acknowledgements

This work was supported by Korea Polar Research Institute (PE19020). The authors appreciate to department of Electronic & Electrical Engineering, University of Bath, U.K. who provide us Esrange meteor radar data and to MLS data supporting team for providing temperature data.

References

Baggaley, W.J., Cummack, C.H., 1974. Meteor train ion chemistry. J. Atmos. Terr. Phys. 36, 1759–1773. https://doi.org/10.1029/1999RS00226.

Ballinger, A.P., Chilson, P.B., Palmer, R.D., Mitchell, N.J., 2008. On the validity of ambipolar diffusion assumption in the polar mesopause region. Ann. Geophys. 26, 3439–3443. https://doi.org/10.5194/angeo-26-3439-2008.

Cevara, M.A., Reid, I.M., 2000. Comparison of atmospheric parameters derived from meteor observations with CIRA. Radio Sci. 35 (3), 833–843. https://doi.org/10.1029/1999RS00226.

Chilson, P.B., Czechowsky, P., Schmidt, G., 1996. A comparison of ambipolar diffusion coefficients in the meteor trains using VHF radar and UV lidar. Geophys. Res. Lett. 23, 2745–2748. https://doi.org/10.1029/96GL02577.

Dyrland, M.E., Hall, C.M., Mulligan, F.J., Tsutsumi, M., 2010. Improved estimates for neutral air temperatures at 90km and 78°N using satellite and meteor radar. Radio Sci. 45, RS4006. https://doi.org/10.1029/2009RS004344.

Dyrud, L.P., Oppenheim, M.M., vom Endt, A.F., 2001. The anomalous diffusion of meteor trail. Geophys. Res. Lett. 28 (14), 2775–2778. https://doi.org/10.1029/2000GL012749.

Hall, C.M., Aso, T., Tsutsumi, M., Höffner, J., Sigernes, F., Holdsworth, D.A., 2006. Neutral air temperatures at 90 km and 70°N and 78°N. J. Geophys. Res. 11, D14105. https://doi.org/10.1029/2005JD006794.

Hall, C.M., Dyrland, M.E., Tsutsumi, M., Mulligan, F.J., 2012. Temperature trends at 90 km over Svalbard, Norway (78°N 16°E), seen in one decade of meteor radar observations. J. Geophys. Res. 117, D08104. https://doi.org/10.1029/2011JD017028.

Hocking, W.K., Thayaparan, T., Jones, J., 1997. Meteor decay times and their use in determining a diagnostic mesospheric temperature-pressure parameter: methodology and one year of data. Geophys. Res. Lett. 24 (23), 2977–2980. https://doi.org/10.1029/97GL03048.

Hocking, W.K., 1999. Temperatures using radar-meteor decay times. Geophys. Res. Lett. 26 (21), 3297–3300. https://doi.org/10.1029/1999GL003618.

Hocking, W.K., 2004. Radar meteor decay rate variability and atmospheric consequences. Ann. Geophys. 22, 3805–3814. https://doi.org/10.5194/angeo-22-3805-2004.

Hocking, W.K., Singer, W., Bremer, J., Mitchell, N.J., Batista, P., Clemesha, B., Donner, M., 2004. Meteor radar temperatures at multiple sites derived with SKiYMET radars and compared to OH, rocket and lidar measurement. J. Atmos. Sol. Terr. Phys. 66 (6–9), 585–593. https://doi.org/10.1016/j.jastp.2004.01.011.

Holdsworth, D.A., Morris, R.J., Murphy, D.J., Reid, I.M., Burns, G.B., French, W.J.R., 2006. Antarctic mesospheric temperature estimation using the Davis MST radar. J. Geophys. Res. 111, D05108. https://doi.org/10.1029/2005JD006589.

Holmen, S.E., Hall, C.M., Tsutsumi, M., 2016. Neutral atmosphere temperature trends and variability at 90 km, 70°N, 19°E, 2003-2014. Atmos. Chem. Phys. 16, 7853–7866. https://doi.org/10.5194/acp-16-7853-2016.

Jee, G., Kim, J.-H., Lee, C., Kim, Y.H., 2014. Ground-based observations for the upper atmosphere at King Sejong Station, Antarctica. J. Astron. Space Sci. 31 (2), 169–176. https://doi.org/10.5140/JASS.2014.31.2.169.

Jones, W., 1991. Theory of diffusion of meteor trains in the geomagnetic field. Planet. Space Sci. 39 (9), 1283–1288. https://doi.org/10.1016/0032-0633(91)90042-9.

Kim, J.-H., Kim, Y.H., Lee, C.S., Jee, G., 2010. Seasonal variation of meteor decay times observed at King Sejong Station (62.22°S, 58.78°W), Antarctica. J. Atmos. Sol. Terr. Phys. 72 (11–12), 883–889. https://doi.org/10.1016/j.jastp.2010.05.003.

Kim, J.-H., Kim, Y.H., Jee, G., Lee, C., 2012. Mesospheric temperature estimation from meteor decay times of weak and strong meteor trails. J. Atmos. Sol. Terr. Phys. 89, 18–26. https://doi.org/10.1016/j.jastp.2012.07.003.

Kozlovsky, A., Lukianova, R., Shalimov, S., Lester, M., 2016. Mesospheric temperature estimation from meteor decay times during Geminids meteor shower. J. Geophys. Res. 121, 1669–1679. https://doi.org/10.1002/2015JA022222.

Lee, C.S., Younger, J.P., Reid, I.M., Kim, Y.H., Kim, J.-H., 2013. The effect of recombination and attachment on meteor radar diffusion coefficient profiles. J. Geophys. Res. 118, 3037–3043. https://doi.org/10.1002/jgrd.50315.

Lee, C., Kim, J.-H., Jee, G., Lee, W., Song, I.-S., Kim, Y.H., 2016. New method of estimating temperatures near the mesopause region using meteor radar observations. Geophys. Res. Lett. 43 https://doi.org/10.1002/2016GL071082.

Lee, C., Jee, G., Kim, J.-H., Song, I.-S., 2018. Meteor echo height ceiling effect and mesospheric temperature estimation from meteor radar observations. Ann. Geophys. 36, 1267–1274. https://doi.org/10.5194/angeo-36-1267-2018.

Lima, L.M., Batista, P.P., Paulino, A.R., 2018. Meteor radar temperatures over the Brazilian low-latitude sectors. J. Geophys. Res. 123 (9), 7755–7766. https://doi.org/10.1029/2018JA025620.

Liu, L., Liu, H., Le, H., Chen, Y., Sun, Y.Y., Ning, B., Hu, L., Wan, W., Li, Na., Xiong, J., 2017. Mesospheric temperatures estimated from the meteor radar observations at Mohe, China. J. Geophys. Res. 122, 2249–2259. https://doi.org/10.1002/2016JA023776.

Meek, C.E., Manson, A.H., Hocking, W.K., Drummond, J.R., 2013. Eureka, 80°N, SKiTMER meteor radar temperatures compared with Aura MLS values. Ann. Geophys. 31, 1267–1277. https://doi.org/10.5194/angeo-3101267-2013.

Schult, C., Brown, P., Pokorny, P., Stober, G., Chau, J.L., 2018. A meteoroid stream survey using meteor head echo observations from the Middle Atmosphere ALOMAR radar system (MAARSY). Icarus 309, 177–186. https://doi.org/10.1016/j.icarus.2018.02.032.

Schwartz, M.J., et al., 2008. Validation of the Aura Microwave Limb sounder temperature and geopotential height measurements. J. Geophys. Res. 113, D15S11. https://doi.org/10.1029/2007D008783.

Singer, W., Bremer, J., Hocking, W.K., Weis, J., Latteck, R., Zecha, M., 2003. Temperature and wind tides around the summer mesopause at middle and arctic latitudes Part 1. Mean temperatures. J. Atmos. Sol. Terr. Phys. 66, 607–616. https://doi.org/10.1016/j.jastp.2004.01.012.

Stober, G., Jacobi, C., Frohlich, K., Oberheide, J., 2008. Meteor radar temperatures over Collm (51.3°N, 13°E). Adv. Space Res. 42 (7), 1253–1258. https://doi.org/10.1016/j.asr.2007.10.018.

Stober, G., Jacobi, C., Singer, W., 2011. Meteoroid mass determination from underdense trails. J. Atmos. Sol. Terr. Phys. 73, 895–900.

Yi, W., Xue, X., Chen, J., Dou, X., Chen, T., Li, N., 2016. Estimation of mesopause temperatures at low latitudes using the Kunming meteor radar. Raido Sci. 51 (3), 130–141. https://doi.org/10.1002/2015RS005722.

Younger, J.P., Reid, I.M., Vincent, R.A., Holdsworth, D.A., 2008. Modeling and observing the effect of aerosols on meteor radar measurements of the atmosphere. Geophys. Res. Lett. 35, L15812. https://doi.org/10.1029/2008GL033763.

Younger, J.P., Lee, C.S., Reid, I.M., Vincent, R.A., Kim, Y.H., Murphy, D.J., 2014. The effects of deionization processes on meteor radar diffusion coefficients below 90 km. J. Geophys. Res. 119, 10,027–10,043. https://doi.org/10.1002/2014JD021787.

Younger, J.P., Reid, I.M., Vincent, R.A., Holdsworth, D.A., Murphy, D.J., 2009. A southern hemisphere survey of meteor shower radiants and associated stream orbits using single station radar observations. Mon. Not. R. Astron. Soc. 398, 350–356. https://doi.org/10.1111/j.1365-2966.2009.15142.x.